Scalable Computing: Practice and Experience, ISSN 1895-1767, http://www.scpe.org
© 2024 SCPE. Volume 25, Issues 5, pp. 3376–3387, DOI 10.12694/scpe.v25i5.3091

A FAULT MONITORING SYSTEM FOR MECHANICAL AND ELECTRICAL EQUIPMENT OF SUBWAY VEHICLES BASED ON BIG DATA ALGORITHMS

GENG LI*, YA LI†, AND HONGXUE BI‡

Abstract. This paper uses big data technology to extract the electromechanical fault characteristics of metro vehicles and analyze the current situation under different fault conditions to ensure the operation quality and safety of metro operations. It also establishes a simulation model to simulate the current waveform of metro vehicles under different fault conditions and analyze the fault phenomenon. The simulation test results show that: (1) The current waveform of a single transistor with the hard fault is compared with the simulated current waveform under a normal state. The upper part of the A phase current waveform is lost when T1 fails. When T2 fails, the current waveform in the lower half of the C phase current is lost. When T3 fails, the upper half of the B phase current waveform is lost. (2) The current waveform in the hard fault's upper and lower bridge arms will have phase loss. In the T25 fault, the C phase current is completely lost. In the T14 fault, the phase A current waveform is completely lost. In the T36 fault, the phase B current is completely lost. (3) The current waveform of a single transistor with a soft fault is complete, but the overall current amplitude is reduced. When a T1 fails, the A phase current tends to rise first and then fall. Compared to normal, the amplitude of the current decreases, and the peak decreases slightly. (4) The current values of phase B and phase C of the two transistors on the same bridge above and below the soft fault are mostly the same. The phase A current output value decreases in both the positive and negative half cycles. This paper aims to improve the monitoring ability of the monitoring system of electromechanical equipment of metro vehicles, which plays a specific role in maintaining the safety of subway operations and improving the quality of subway operations.

Key words: Big data technology, metro vehicles, electromechanical equipment, monitoring systems, simulation

1. Introduction.

With the development of urbanization, the role of urban rail transit in cities is becoming increasingly important. The metro is the backbone of public transportation in modern large cities and the backbone of passenger transportation within the city [1,2]. Metro vehicle Electromechanical Equipment (EE) is a general term for electrical and mechanical equipment that converts electricity and other energy. It is indispensable equipment for maintaining metro operations. The failure of electrical equipment in a metro train will directly affect the operational safety of the city's rail vehicles. Therefore, fault monitoring of electrical equipment in metro trains is critical. The converter is the core component of controlling multiple components in the metro electrical equipment. Monitoring the condition of the converter can prevent possible electromechanical failures during metro operation.

At the end of the last century, big data technology began to develop. Big data has a wide range of applications, for example, in healthcare. Analyzing big data through machine learning can help evaluate large amounts of complex healthcare data to improve medical diagnosis and disease classification [3]. During the 13th Five-Year Plan period, big data technology was widely used in urban rail transit. Through big data analysis, South Korea could review the operation of express trains and detect the trend of train traffic [4]. Big data analysis can plan metro travel routes [5]. Advanced big data technology can detect defects in metro tunnels [6]. In terms of metro operation, based on big data technology, an automatic toll collection system with stable system operation, relatively small memory, fast response speed, and low delay can be designed to improve the convenience of residents' lives and accelerate the process of urban construction [7]. Using big data technology can realize the intelligent management of metro operations, which plays a vital role in alleviating traffic congestion, reducing traffic accidents, and reducing energy consumption [8,9]. In addition, in terms of electromechanical fault detection, the detection system can be highly adaptable based on big data technology.

*Zhengzhou CSCEC Shenzhen Railway Rail Transit Co., Ltd, Zhengzhou, 450000, China (Corresponding author, GengLi2@126.com)
†Zhengzhou CSCEC Shenzhen Railway Rail Transit Co., Ltd, Zhengzhou, 450000, China (YaLi381@163.com)
‡Zhengzhou Railway Vocational & Technical College, Zhengzhou, 450000, China (HongxueBi@126.com)

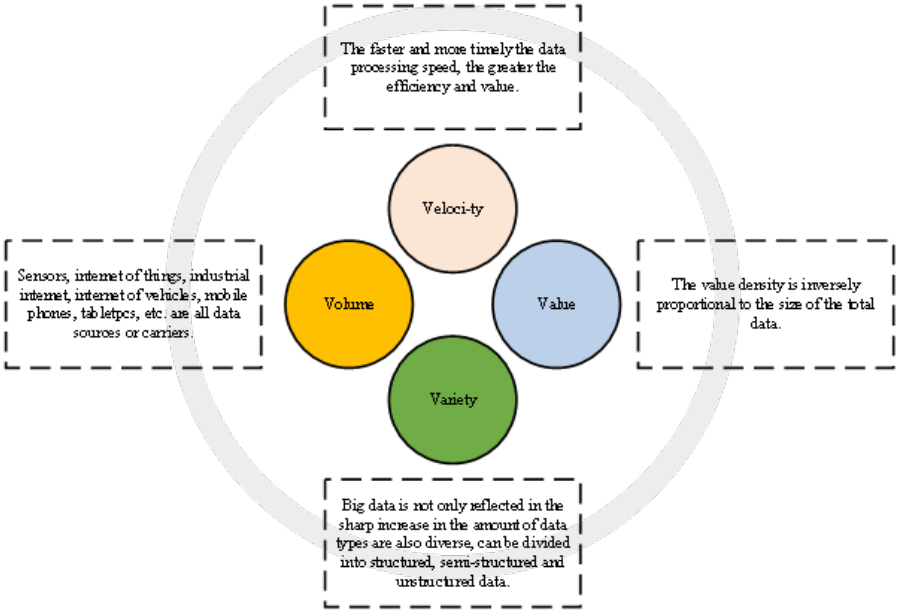

Fig. 2.1: Characteristics of big data technology

It can predict the early electromechanical failure of the aircraft and improve the fault diagnosis performance of the electromechanical system [10,11]. When dealing with complex classification problems, the use of big data technology can realize real-time fault detection of key components of the electromechanical traction system of high-speed trains, which is of great significance for improving the reliability of train motors and reducing the cost of support [12,13]. Electromechanical faults can be monitored using big data technology to establish simulation models.

Firstly, this paper uses big data technology to extract the electromechanical fault characteristics of metro vehicles and analyze the current situation under different fault conditions to ensure the operation quality and safety of metro operation and improve the monitoring of metro EE. Secondly, a simulation model is established to simulate the current waveform of metro vehicles under different fault conditions and analyze the fault phenomenon. The innovation point is to combine big data technology with the electromechanical fault monitoring system of metro vehicles and analyze the current waveform of the converter under different faults through simulation models. The monitoring of EE of metro vehicles has been improved, which has played a specific role in maintaining the safety of metro operations.

2. Establishment of the electromechanical fault simulation model for metro vehicles.

2.1. Big Data Technology. Big data technology refers to the application technology of big data, including various big data platforms, big data index systems, and big data application technology . As one of the leading development directions in the information field, big data technology can be applied to data mining, data analysis, and data sharing in massive data. It leverages the potential value of data to create substantial economic benefits. Big data can optimize resource utilization while making informed decisions [14,15]. In the oil and gas industry, big data technology can be used to analyze seismic and microseismic data, reduce drilling time and improve drilling safety, optimize the performance of production pumps, improve asset management, and improve transportation safety [16,17]. Big data technology can promote students' interest in learning and improve their concentration on learning in college education . Big data management in big data technology can organize and analyze mining data well. Big data technology is one of the promising technologies that could reshape the entire mining landscape .

The characteristics of big data technology are shown in Figure 2.1.

Big data technology has many data processing methods, such as Bayesian networks, random forests, decision trees, Principal Component Analysis (PCA), Gaussian mixture models, and regression analysis models. Here, the PCA and the Weibull distribution method are mainly used for data preprocessing.

PCA is a statistical method that can comprehensively analyze the problem, save calculation time and cost by reducing the dimensionality of the data set, and improve the accuracy of the calculation. As a basic mathematical analysis method, PCA has applications in the fields of demographics, quantitative geography, mathematical modeling, and mathematical analysis. It is a commonly used multivariate analysis method. PCA has three main functions: reducing the dimensionality of the data space, analyzing the relationship between variables, and using graphics to represent multidimensional data.

Suppose $X_1, X_2, ..., X_i (i = 1, 2, ..., j)$ is the eigenvector corresponding to the eigenvalues of the covariance matrix of M. $M_1, M_2, ..., M_i (i = 1, 2, ..., j)$ is the normalized value of the original variable. Then, the following relationship exists when normalizing.

$$F = X_1 * M_1 + X_2 * M_2 + ... + X_i * M_i \tag{2.1}$$

The Weibull distribution method is the theoretical basis of reliability analysis. It is suitable for inferring the wear of electromechanical products, industrial manufacturing, predicting the weather, predicting technological changes, and modeling the received clutter signal. The Weibull distribution method was proposed in 1927 and explained in detail by the Swedish engineer and mathematician Waloddi Weibull in 1951. According to the form, it can be divided into three types: the one-parameter Weibull distribution, the two-parameter Weibull distribution, and the three-parameter Weibull distribution or mixed Weibull distribution.

The Weibull distribution is a continuous probability distribution. Suppose x is a random variable, y>0 is the scale parameter, and z>0 is the shape parameter. When z=1, the probability density function is an exponential distribution; when z=2, it is a Rayleigh distribution. The probability density is calculated as follows.

$$f(x, y, z) = \begin{cases} \frac{z}{y}(\frac{x}{y})^{z-1}, x \geqslant \\ 0, x < 0 \end{cases} \tag{2.2}$$

γ is the gamma function, and the mean is calculated according to Eqaution 2.3.

$$E = y\gamma(1 + \frac{1}{z}) \tag{2.3}$$

If the time is t, m is the standard parameter, and s is the positional parameter. Then, the continuous distribution function f(x) is:

$$f(t) = \frac{z}{m}(\frac{1-s}{z})^{Z-1} E^{-(\frac{t-s}{m})^Z} \tag{2.4}$$

2.2. Metro EE. Metro EE is mainly divided into ventilation and air conditioning systems, water supply and drainage systems, power lighting systems, elevator and screen door systems, automatic ticket vending systems, power supply systems, communication signals and other weak current systems, civil air defense projects, and subway vehicles [18,19]. Metro trains mainly use automation equipment with electronic computer processing technology as the core. The role of this equipment is to replace manual labor with mechanized and electrified systems to ensure the operation and safety of trains. Metro trains mainly include car bodies, power bogies and non-power bogies, traction buffer connection devices, brake devices, current receiver devices, internal vehicle equipment, and electrical systems. Among them, the electrical system is divided into the main, auxiliary, and electronic and control circuits. Converters are auxiliary circuit systems.

The characteristics of EE failures are the characteristics of the occurrence, development, and change of faults in a complete life cycle of EE from use to no longer use. Figure 2.2 shows the classification of fault characteristics of EE.

The auxiliary power supply system of the metro train receives the current of the high-voltage power supply network. These currents are transmitted by a pantograph or a third rail catenary. The controller controls the inverter circuit. The voltage on the catenary of the auxiliary inverter is changed to a medium-pressure flow.

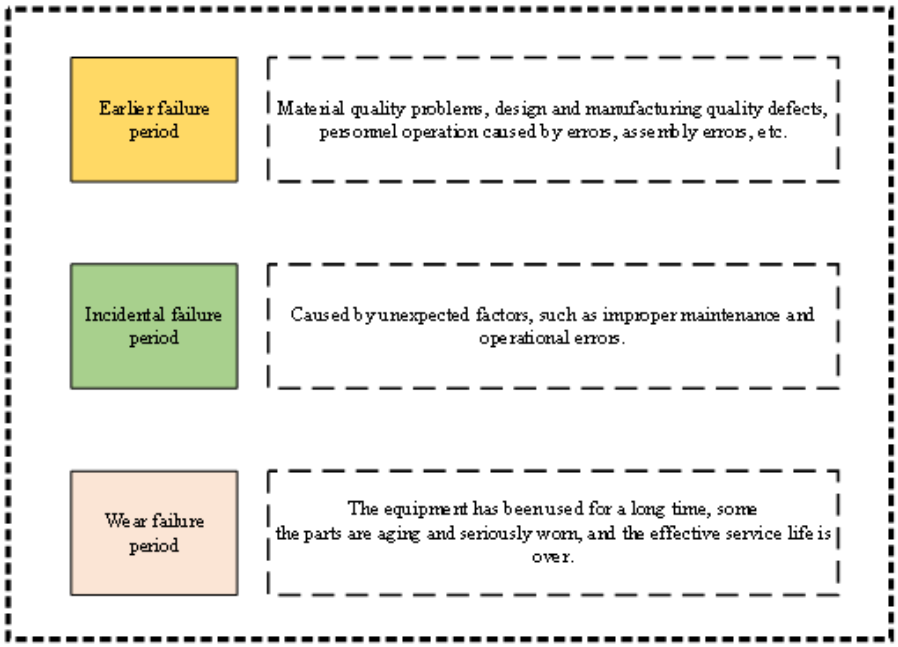

Fig. 2.2: Classification of electromechanical fault characteristics

The auxiliary power supply system is divided into the grid-connected, cross-power, and extended power supply. A bus bar connects the grid-connected power supply to the whole vehicle. There is no contactor in the middle, and the two auxiliary inverters work together. The cross-power supply is the direct power supply from the busbar to the trunks that have been grouped. Under normal circumstances, the vehicle alternating current load is divided into two groups on average according to the equipment's power. Two auxiliary inverters supply power to each of the two sets of equipment. The extended power supply is a more complex way of supplying power to two independent units using a bus bar. There is a contactor between the two auxiliary inverters. When the contactor is turned off, the malfunctioning auxiliary inverter stops working, and another auxiliary inverter is responsible for the entire vehicle.

Among them, the power supply switching mode of cross-power and grid-connected power supply is the simplest, and no additional hardware is required. When switching the expansion circuit, it is necessary to set up the expansion contactor, and the auxiliary inverter must also stop working.

The specific power supply system load is presented in Figure 2.3.

The fault characteristics extraction of the metro electrical system can be carried out through three aspects: time domain, frequency domain, and time-frequency domain. The time domain mainly describes the relationship of mathematical functions or physical signals to time. Time is the independent variable, and signal change is the dependent variable. Time domain analysis uses the time axis as the coordinate to represent dynamic signal changes. The frequency domain is a coordinate system used to describe the frequency characteristics of a signal. The independent variable is the frequency, and the dependent variable is the change amplitude of the frequency signal. It is also a spectrogram, which describes the frequency structure of the signal and the relationship between the frequency and the amplitude of the frequency signal, mainly used in electronics, control system engineering, and other aspects. The time-frequency domain combines time and frequency to express information about frequency over time. The time domain process is straightforward, and the frequency domain process needs to be transformed. The time-frequency domain process is more complex, but the resulting signal quality is higher. Therefore, the fault characteristics of the metro electrical system are extracted from the perspectives of time-frequency and time domains.

Time-domain fault feature extraction is to count the different feature manifestations of signals in different

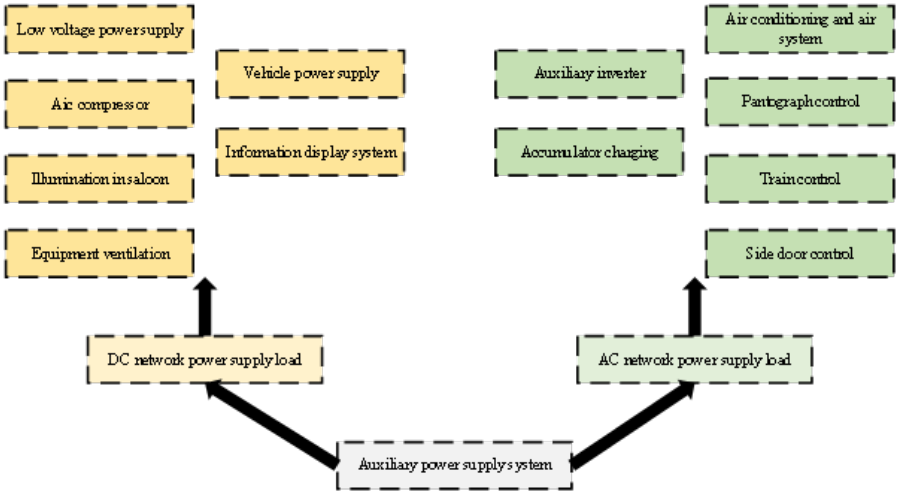

Fig. 2.3: Auxiliary power supply system load

states in the time domain. There are two main indicators of time-domain signals: dimensioned and dimensionless parameters. Dimensioned parameters have unit values and are easily affected by environmental interference. Dimensionless parameters are values without units and are not affected by interference factors.

Dimensioned parameters are calculated according to Eqaution 2.5-Eqaution 2.7.

$$A = \int_{-\infty}^{\infty} AP(A)dx \tag{2.5}$$

$$\alpha = \int_{-\infty}^{\infty} A^3 P(A)dx \tag{2.6}$$

$$\beta = \int_{-\infty}^{\infty} A^4 P(A)dx \tag{2.7}$$

In Equation 2.5-2.7, P(A) is the probability density function, A is the mean of any sample, α is the degree of skewness, and β is the steepness.

Dimensionless parameters are calculated according to Eqaution 2.8-Eqaution 2.10.

$$X = \frac{A_{RMS}}{|\overline{A}|} \tag{2.8}$$

$$L = \frac{A_{MAX}}{A_{RMS}|} \tag{2.9}$$

$$K = \frac{e[(A-U)^4]}{\sigma^4} \tag{2.10}$$

In Eqaution 2.8-Equation 2.10, U is the mean, U^4 is the fourth-order center distance of the random variable A, e is the expectation, A_{RMS} is the square root of the mean, σ is the standard deviation, X is the waveform index, L is the peak indicator, and K is the steepness factor.

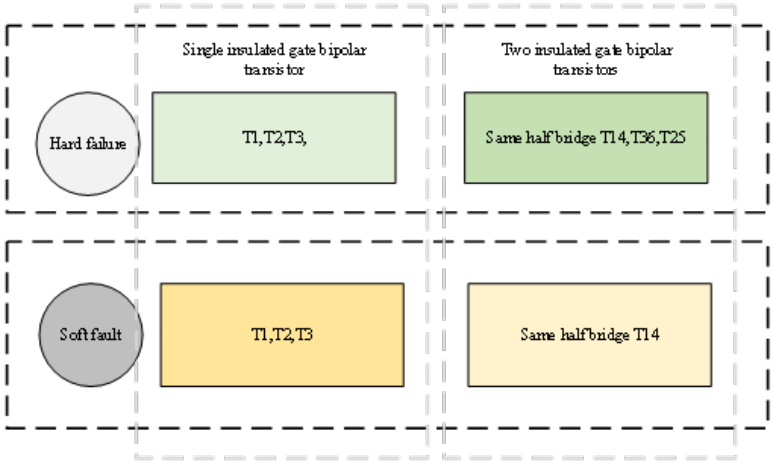

Fig. 2.4: Electrical system fault classification

Time-frequency domain fault feature extraction uses Short-time Fourier Transform (STFT), S transform, Empirical Mode Decomposition (EMD), and other methods to extract signals.

The STFT refers to a mathematical transformation related to the Fourier transform to determine the frequency and phase of a sine wave in the local area of a time-varying signal. The uncertainty criterion limits the STFT window function, and the area of the time-frequency window is not less than two. Therefore, the time and frequency resolution of the STFT window function cannot be optimized simultaneously.

The S transform replaces wavelet basis functions with Gaussian windows. It is also known as the "phase orthogonal" continuous wavelet transform. The signal is divided into many small time intervals, and each time interval is analyzed with the Fourier transform to determine the frequency at which the time interval exists. The feature quantity extracted by the S transform is not sensitive to noise.

EMD is a novel adaptive signal processing method for nonlinear and nonstationary signals. It decomposes the signal based on the timescale characteristics of the data itself. It does not require pre-setting. Compared with the previous two methods, the data of EMD is more intuitive.

Figure 2.4 demonstrates the fault classification of the metro electrical system.

2.3. Simulation model establishment. Matrix Laboratory (MATLAB) simulation tool is a commercial mathematical software produced by MathWorks in the United States. It is mainly used in data analysis, deep learning, control system design and simulation, data image processing, and data signal processing. MATLAB, along with Mathematica and Maple, is known as the three major mathematical software. MATLAB integrates matrix calculations, numerical analysis, modeling and simulation of nonlinear dynamic systems, and scientific data visualization in an easy-to-use windowed environment, largely freeing itself from the editing mode of traditional non-interactive programming languages.

The advantage of MATLAB is its efficient numerical and symbolic computing capabilities. It can handle complex and tedious mathematical operations. It has complete graphics processing functions to visualize calculation results. MATLAB also has a feature-rich toolkit that simplifies data processing.

MATLAB has five major system structures: development environment, mathematical library, language, graphics processing system, and application programming interface. The specific system structure is shown in Figure 2.5.

With the help of the Simulink module in the MATLAB tool, simulation models of auxiliary inverter circuits can be built. The simulation model is divided into two inverter modules: the inverter control module and the inverter output module.

Pulse-width modulation control is implemented in the inverter control module using the pulse-width modulation generator in the module library. The input of the pulse-width modulation generator is set with a sine

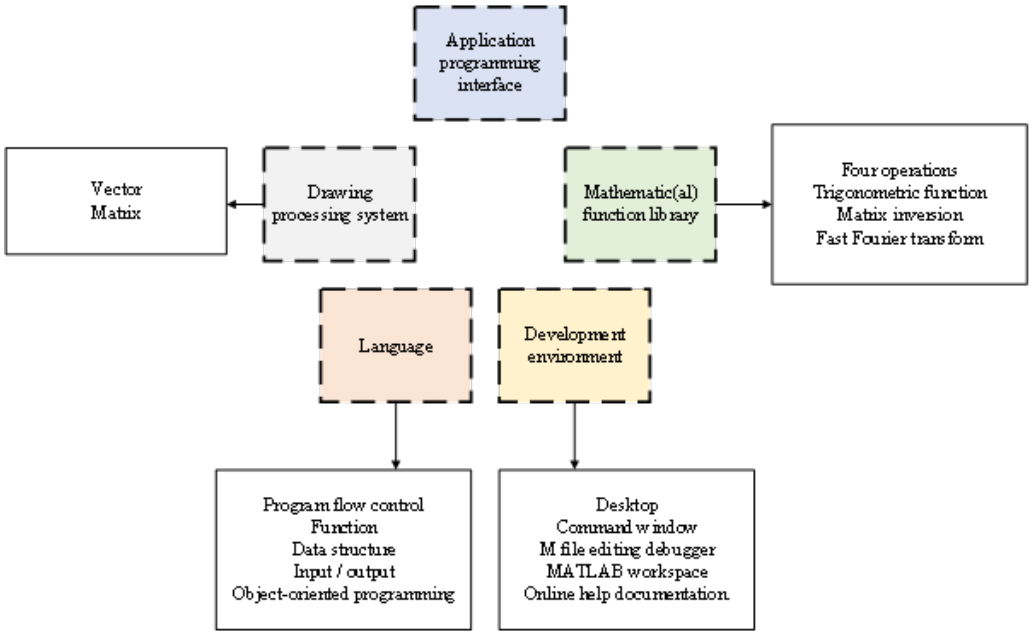

Fig. 2.5: MATLAB system structure

wave with a difference of 120° to control the Insulated Gate Bipolar Transistor (IGBT). The generator output is connected to the gate. It is necessary to prevent the reduction of harmonic content and power life problems of the inverter simulation output voltage caused by the excessive switching frequency of the components in the actual experiment. Therefore, the carrier frequency in the pulse generator is set to 0.6, the modulation wave frequency is set to 50, and the generation period mode is selected as the 3-arm bridge of six pulses.

In the inverter output module, the main circuit is set as a three-phase bridge inverter circuit. IGBT modules include gates, collectors, generators, module test terminals, and module monitoring terminals. The internal resistor size is set to 0.02Ω, and every six IGBT modules form a complete three-phase bridge inverter circuit.

A filter circuit that combines inductors and capacitors is built using modules in the component library. The input voltages of interfaces one, two, and three at the left end are set to the output voltage of the inverter circuit, and the output voltages of four, five, and six after the interface at the right end are set to sine waveforms.

In the simulation model, the grid voltage output of the auxiliary inverter system is set to 1,500V. The direct current voltage changes from 300V to 600V through the battery circuit and resonant converter. In the simulation experiment, the maximum voltage is selected as the input voltage value, set to a purely resistive load. The resistor size is 0.6, the total simulation time is 0.1 seconds, and waveforms are recorded every 0.01 seconds. The output of the simulation circuit is given in Figure 2.6.

3. Simulation results of electromechanical faults of metro vehicles.

3.1. Hard fault simulation results. The variation in the current waveform of a single insulated-gate bipolar transistor is shown in Figure 3.1.

From Figure 3.1, when the power tube T1 fails, the current fluctuation range of phase A is between 0 and -400A, the upper part is lost, and the changing trend will repeat every 0.02s. Phase B current fluctuates from 300 to -300A. The current change showed a trend of increasing first and then decreasing, repeating every 0.02s and five times within 0.1s. The C phase current range and repetition are consistent with the B phase current, but the trend is first falling and then rising. When the power tube T2 fails, the current change trend of phase A is first increasing and then decreasing, and it repeats every 0.02s. The current varies from 300 to -300A. The current change trend of phase B is first falling and then rising, which coincides with the phase A current about every 0.01s. The current varies from 300 to -400A. The C-phase current varies from 400 to 0A. The

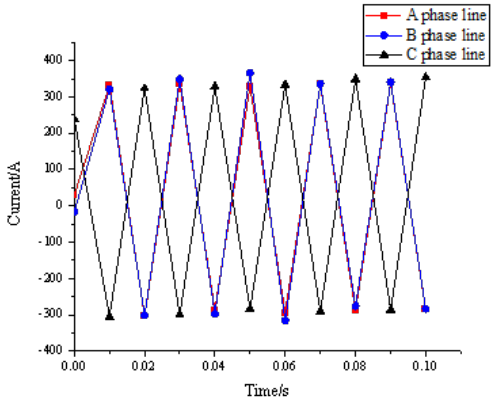

Fig. 2.6: Output of simulation circuit

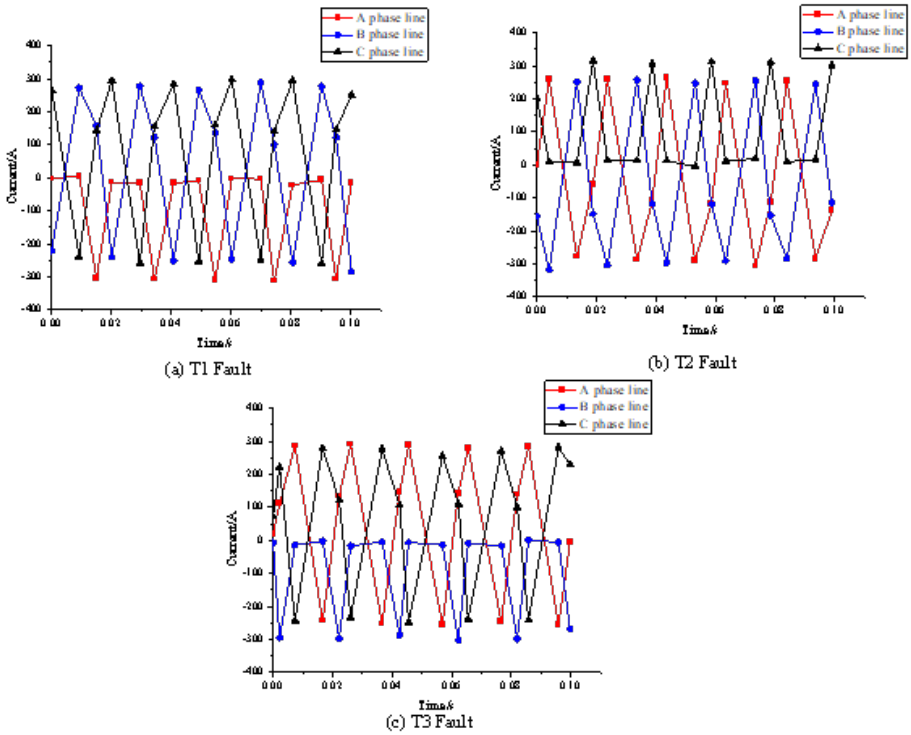

Fig. 3.1: Change in the current waveform of a hard-faulted single-insulated-gate bipolar transistor

current coincides every 0.02s, and the lower half of the current waveform is lost. When the T3 fault occurs, the current trend of phase A is consistent with that of the T2 fault. The specific current values are slightly different, but the overall range is the same. The waveform in the upper half of the phase B current is lost, and the current trend is first to fall and then rise. After rising, the current value remains 0.01s and drops again, and the consumption time of each process is about 0.02s. The trend of the current change in phase C is similar to the change in phase C at the T1 fault. In general, compared with the simulated current waveform under normal conditions, waveform loss of different phases will occur under different faults. The fault type can be

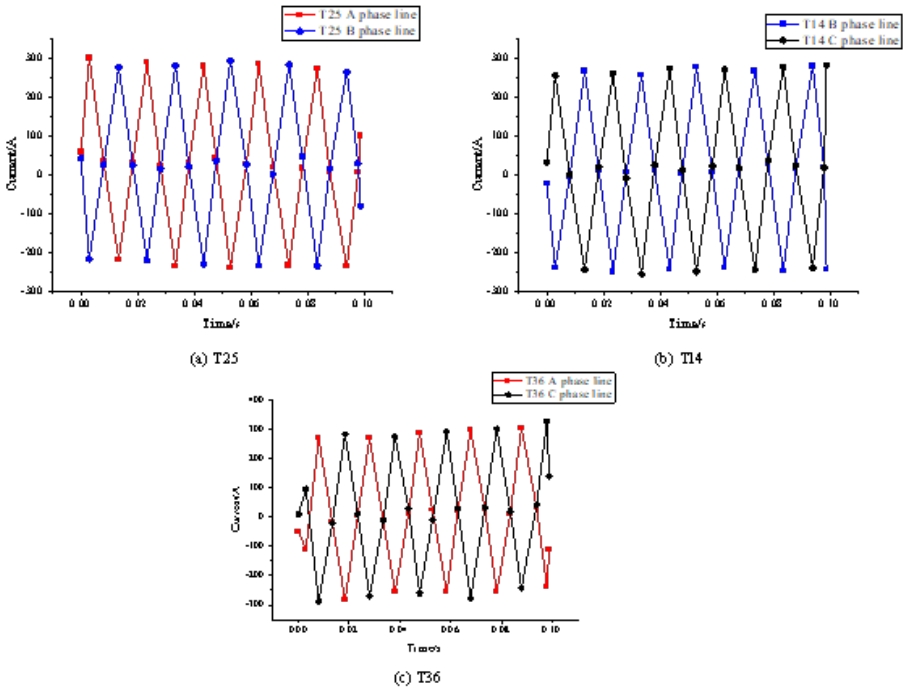

Fig. 3.2: Changes in current waveforms of two insulated-gate bipolar transistors on the upper and lower legs of a hard fault

reversed according to the waveform loss.

The current waveforms of the two insulated-gate bipolar transistors are plotted in Figure 3.2.

From Figure 3.2, in both transistor faults on the upper and lower bridge arms, the T25 fault shows only phase A current and phase B current, and the phase C current is completely lost. Phase A's current trend is first up and then down, and the current range is between 300 and -250A. There is no waveform loss. The current trend of phase B is completely opposite to the current trend of phase A. The current range of both is consistent, and the waveform is complete. In the T14 fault, only the B phase current and the C phase current are present, and the A phase current waveform is completely lost. The current trend of phase B is consistent with the current trend of phase B of the T25 fault, but the lower limit of the variation range is slightly lower than that of the T25 fault. The current trend of phase C is first rising and then decreasing. The overall current range is approximately 250 to -250A, and the waveform is complete. In the T36 fault, the A phase current and C phase current remain intact, and the B phase current is completely lost. Phase A's current change trend is to decline and then rise. The current variation range is about 300 to -300A, with large fluctuations in the middle. The current trend of phase C is first increasing and then decreasing, the lower limit of the current range exceeds -300A, and the waveform is complete. In general, the current waveform in the fault of the upper and lower bridge arms will have phase loss, and the phase loss of different power tubes will be different. In real circuits, this type of fault will cause a current short circuit.

3.2. Soft fault simulation results. The variation in the current waveform of a single insulated-gate bipolar transistor is revealed in Figure 3.3.

From Figure 3.3, in soft faults, resistance is mainly considered. At a thermally stable operating temperature of 30°C, the thermally stable resistance exceeds 0.004Ω. When a T1 fault occurs, the current in phase A tends to rise first and then fall. The current range is between 300 and -300A. Compared to normal, the amplitude of the current decreases, and the peak decreases slightly. The current trend of phase B is opposite to the current trend of phase A. The current range is consistent. The current amplitude is small compared to the simulated

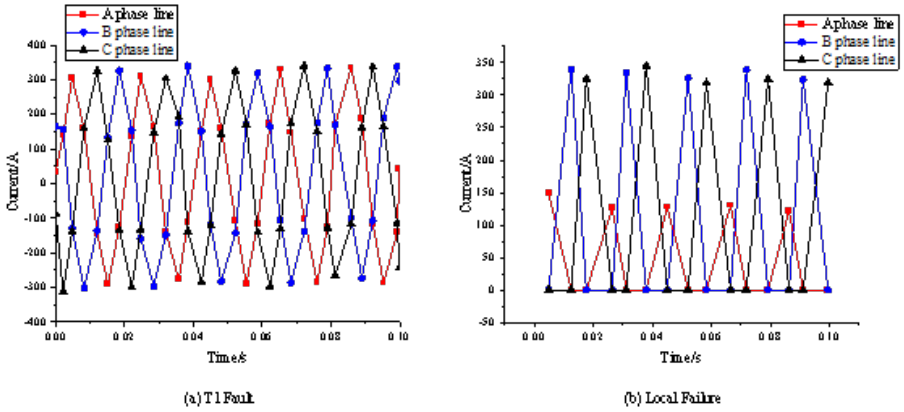

Fig. 3.3: Variation of the current waveform of a soft-faulted single-insulated-gate bipolar transistor

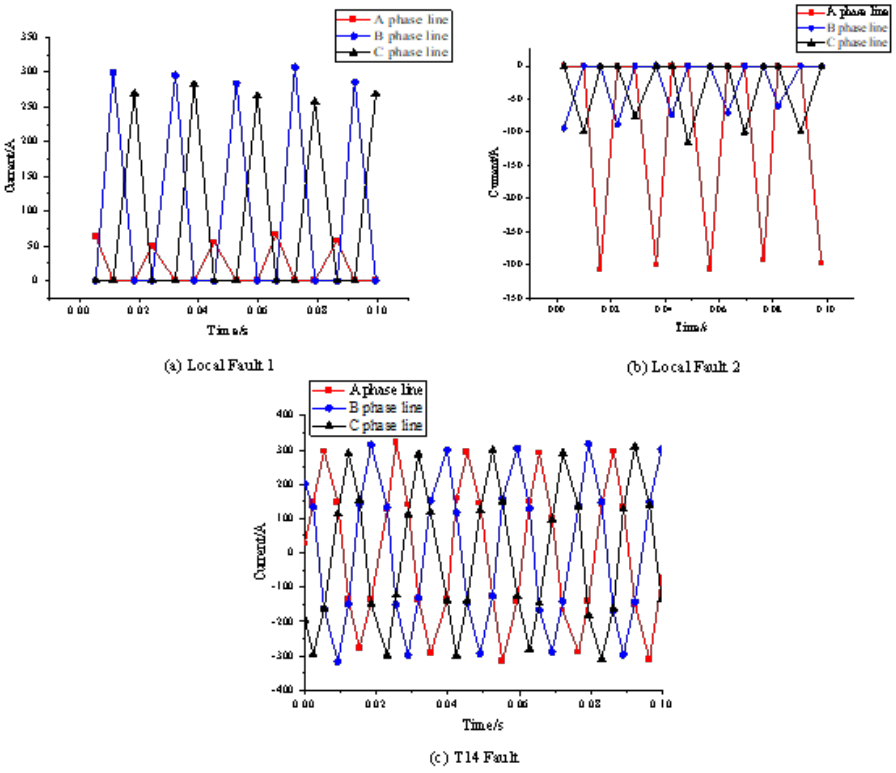

Fig. 3.4: Changes in current waveforms of two insulated-gate bipolar transistors with the same bridge above and below the soft fault

current waveform under normal conditions. The current variation trend of phase C is quite different from that of the simulation circuit under normal conditions, and the lowest value occurs when it is close to 0.02s. Overall, the soft-fault single transistor current waveform is intact, but the overall current amplitude is reduced.

The current waveforms of the two insulated-gate bipolar transistors are shown in Figure 3.4.

From Figure 3.4, when both transistors on the same bridge of the soft fault have a fault problem, the

current change trend of phase A increases first and then decreases, which is similar to the waveform of a single transistor with a soft fault[20]. Phase A currents range from 300 to -300A. Compared to the simulated current waveform under normal conditions, the current output value decreases in both the positive and negative half cycles. The current trend of phase B is completely opposite to the current trend in normal conditions. The current trend of the C phase is consistent with the case of a soft fault single transistor, and the current value at 0s is slightly different. On the whole, the current value of phase A of the two transistors with the same bridge above and below the soft fault will decrease, and the current value of phase B and phase C will not change much.

4. Conclusion. In this paper, the electromechanical fault characteristics of metro vehicles are extracted by big data technology, and the current situation under different fault conditions is analyzed. The simulation model is established. Additionally, the Simulink module in the MATLAB tool is used to simulate the current waveform of metro vehicles under different fault conditions and analyze the hard and soft fault phenomena. The simulation results show that: (1) The current waveform of a single transistor with the hard fault is compared with the simulated current waveform under a normal state. Waveform loss of different phases occurs under different fault conditions. The fault type can be reversed according to the waveform loss. When power tube T1 fails, the upper half of the phase A current waveform is lost. When the power tube T2 fails, the C-phase current coincides every 0.02s, and the lower half of the current waveform is lost. When T3 fails, the waveform in the upper half of the B phase current is lost. The current trend is first to fall and then rise, and the consumption time of each process is about 0.02s. (2) The current waveform in the hard fault's upper and lower bridge arms will have phase loss, and the phase loss of different power tubes is different. At the T25 fault, only phase A current and phase B current are shown, and phase C current is completely lost. In the T14 fault, only the B phase current and the C phase current are present, and the A phase current waveform is completely lost. In the T36 fault, the A and C currents remain intact, and the B phase current is completely lost. (3) The current waveform of a single transistor with a soft fault is complete, but the overall current amplitude is reduced. When T1 fails, the current trend of phase A rises first and then falls. Compared to normal, the amplitude of the current decreases, and the peak decreases slightly. The current trend of phase B is opposite to the current trend of phase A. The current variation trend of phase C is quite different from that of the simulation circuit under normal conditions, and the lowest value occurs when it is close to 0.02s. (4) The current value of phase A of the two transistors on the same bridge of the soft fault will decrease, and the current value of phase B and phase C will not change much. The current trend of phase A is to increase first and then decrease. Compared to the simulated current waveform under normal conditions, the current output value decreases in both the positive and negative half cycles.

The disadvantage is that the simulation model only studies the current waveforms of the two IGBTs on the upper and lower bridge arms of the hard fault and the upper and lower bridges of the soft fault. It does not consider the current waveforms of the two IGBTs under the same half-bridge and the cross half-bridge. The research on converter faults still needs to be completed. Furthermore, there is the problem of short simulation experiment time. In subsequent research, converter faults under different conditions can be added, the simulation time can be extended, and a more comprehensive study can be carried out. The electrical system faults can be inferred from different current waveforms to enrich the fault types, thereby enhancing the monitoring ability of the electromechanical fault system. The fault model of the transformer of the electrical system of EE of metro vehicles established by big data technology improves the monitoring ability of transformer faults of the metro electrical system. It also plays a specific role in improving the performance of the monitoring system of EE of metro vehicles, enhances the safety of metro operation and the quality of metro operation, and contributes to the development of urban rail transit.

REFERENCES

[1] Liu Z., Li Y., Zhao L., et al. (2021) Construction of intelligent query system for metro electromechanical equipment faults based on the knowledge graph[J]. Journal of Intelligent & Fuzzy Systems, 41(3), 4351-4368.

[2] Li S., Wei X., Zhang Z., et al. (2019) Subway Station Capacity Maintained by Optimizing a Maintenance Schedule of Key Equipment[J]. Applied Sciences, 9(7), 1386.

[3] Ngiam K. Y., Khor W. (2019) Big data and machine learning algorithms for health-care delivery[J]. The Lancet Oncology, 20(5), e262-e273.
[4] Yonghyun L., Minhyuk K., Jisoo K., et al. (2021) An exploratory study on the effectiveness verification and alternatives to improve the congestion level of subway line 9[J]. IJEMR, 5(4), 1-5.
[5] Park S. T., Kim Y. K. (2019) A study on deriving an optimal route for foreign tourists through the analysis of big data[J]. Journal of Convergence for Information Technology, 9(10), 56-63.
[6] Wang A., Togo R., Ogawa T., et al. (2022) Defect detection of subway tunnels using advanced U-Net network[J]. Sensors, 22(6), 2330.
[7] Huang K., Lu S., Li X., et al. (2022) Predicted Mean Vote of Subway Car Environment Based on Machine Learning[J]. Big Data Mining and Analytics, 6(1), 1-14.
[8] Welch T. F., Widita A. (2019) Big data in public transportation: a review of sources and methods[J]. Transport reviews, 39(6), 795-818.
[9] Yin Z., Hu N., Chen J., et al. (2022) A review of fault diagnosis, prognosis and health management for aircraft electromechanical actuators[J]. IET Electric Power Applications, 16(11), 1249-1272.
[10] Dalla Vedova M. D. L., Germanà A., Berri P. C., et al. (2019) Model-based fault detection and identification for prognostics of electromechanical actuators using genetic algorithms[J]. Aerospace, 6(9), 94.
[11] Liu Z. H., Lu B. L., Wei H. L., et al. (2019) Fault diagnosis for electromechanical drivetrains using a joint distribution optimal deep domain adaptation approach[J]. IEEE Sensors Journal, 19(24), 12261-12270.
[12] Arellano-Espitia F., Delgado-Prieto M., Martinez-Viol V., et al. (2020) Deep-learning-based methodology for fault diagnosis in electromechanical systems[J]. Sensors, 20(14), 3949.
[13] Li Y. (2022) Exploring real-time fault detection of high-speed train traction motor based on machine learning and wavelet analysis[J]. Neural Computing and Applications, 34(12), 9301-9314.
[14] Kushwaha A. K., Kar A. K., Dwivedi Y. K. et al. (2021) Applications of big data in emerging management disciplines: A literature review using text mining[J]. International Journal of Information Management Data Insights, 1(2), 100017.
[15] Wang J., Yang Y., Wang T., et al. (2020) Big data service architecture: a survey[J]. Journal of Internet Technology, 21(2), 393-405.
[16] Price W. N., Cohen I. G. (2019) Privacy in the age of medical big data[J]. Nature medicine, 25(1), 37-43.
[17] Mohammadpoor M., Torabi F. (2020) Big Data analytics in oil and gas industry: An emerging trend[J]. Petroleum, 6(4), 321-328.
[18] Yang C., Huan S., Yang Y., et al. (2020) Application of big data technology in blended teaching of college students: a case study on rain classroom[J]. International Journal of Emerging Technologies in Learning (iJET), 15(11), 4-16.
[19] Qi C. (2020) Big data management in the mining industry[J]. International Journal of Minerals, Metallurgy and Materials, 27(2), 131-139.
[20] Qi H., Chen G., Ma H., et al. (2022) A Subway Sliding Plug Door System Health State Adaptive Assessment Method Based on Interval Intelligent Recognition of Rotational Speed Operation Data Curve[J]. Machines, 10(11), 1075.

Edited by: B. Nagaraj M.E
Special issue on: Deep Learning-Based Advanced Research Trends in Scalable Computing
Received: Dec 28, 2023
Accepted: Mar 20, 2024